Appendix: Scale-by-Scale Analysis and Fractal Cloud Models

A. Marshak and A.B. Davis

A.1 Scale-by-Scale Analysis

Geophysical systems in general, and clouds in particular, exhibit structure over a wide range of scales and have high levels of variability. Thus, to better understand cloud structure, we compile statistical information on a scale-by-scale basis and seek simple connections that relate properties at one scale to another. Based on the turbulent nature of clouds and following a well-established tradition in turbulence study, we seek power laws in the scale parameter, r. The physical meaning of a statistical power law in r is that the same physical processes dominate over a wide range of scales. Smaller parts of the system therefore look like scaled-down versions of larger parts, and vice versa. The most important quantity is then the exponent of the power law. A power-law statistic r^{α} is invariant under a change of scale $r \rightarrow \lambda r$ in the sense that only the scale ratio λ and the exponent α are required to predict the new value. Observation of a power law therefore reflects a statistical invariance under change of scale, called "scale-invariance" or just "scaling." In practice, this means linear relations in log(statistic) – log(scale) plots.

A.1.1 Wavenumber Spectrum and Autocorrelation Function

Let us assume that we have a stochastic process $\phi(x), 0 \leq x \leq L$ and let $\widetilde{\phi}(k), -\infty < k < \infty$ be its Fourier transform. The wavenumber (or energy, or power) spectrum (or spectral density) $E(k)$ of ϕ is defined as

$$E(k) = \frac{1}{L}\langle|\widetilde{\phi}(k)|^2 + |\widetilde{\phi}(-k)|^2\rangle,\ k > 0\ , \tag{A.1}$$

where $\langle\cdot\rangle$ designates ensemble averaging, i.e., over all possible realizations of ϕ. For scale-invariant processes, the wavenumber spectrum follows a power law

$$E(k) \propto k^{-\beta} \tag{A.2}$$

over the large range of wavenumbers $k = 1/r$. The spectral exponent β contains valuable information on the variability in ϕ.

For a real stationary process, a power spectrum can be obtained from a cosine transform of its autocorrelation (e.g., Papoulis, 1965, p. 338),

$$E(k) = 2\int_0^\infty \cos(2\pi kr)\, G(r)\, \mathrm{d}r \tag{A.3}$$

where

$$G(r) = \langle\phi(x + r)\,\phi(x)\rangle \tag{A.4}$$

is the autocorrelation function (assuming $\langle\phi(x)\rangle = 0$). The stationarity assumption translates here in finding no dependence of $\langle\phi(x + r)\,\phi(x)\rangle$ on x upon ensemble averaging. Conversely, we have

$$G(r) = 2\int_0^\infty \cos(2\pi kr)\, E(k)\, \mathrm{d}k\ . \tag{A.5}$$

Note that

$$\langle|\phi^2(x)|\rangle = G(0) = 2\int_0^\infty E(k)\, \mathrm{d}k\ . \tag{A.6}$$

Finally, it follows from (A.4) that

$$\langle[\phi(x + r) - \phi(x)]^2\rangle = 2[G(0) - G(r)] \geq 0\ . \tag{A.7}$$

So if the autocorrelation function $G(r)$ is continuous at $r = 0$, process $\phi(x)$ is stochastically continuous, meaning that (A.7) goes to 0 with r.

For real measurements, we generally have only a small number of "realizations" with a finite spatial sampling,

$$\phi_i = \phi(x_i), x_i = il\ (i = 1, 2, \ldots, N)\ , \tag{A.8}$$

where $N = L/l$ is the total number of points, L the spatial length of record, and l the step size. Let us for simplicity assume that N is a power of 2, and denote the discrete Fourier transform of the data in (A.8) as

$$\widetilde{\phi}_{\pm j} = \widetilde{\phi}(\pm k_j),\ k_j = \frac{j}{L}\left(j = 0, 1, \ldots, \frac{N}{2}\right)\ . \tag{A.9}$$

The associated energy density, as a discrete counterpart of (A.1) is

$$E(k_j) = \frac{2}{L}|\widetilde{\phi}_j|^2, \left(j = 1, 2, \ldots, \frac{N}{2} - 1\right) \tag{A.10}$$

since $\widetilde{\phi}_{-j} = \widetilde{\phi}^*_{+j}$ for real data in (A.8).

Now plotting $N/2 - 1$ values of $E(k_j)$ versus k_j in a log-log plot gives us an estimate of a slope β. However, without a judicious weighting scheme, a least square fit to the power-law in form (A.2) on a log E versus log k plot will be dominated by the smallest scales r (largest wavenumbers k). The contribution of large scales to the exponent β becomes virtually nil. To make all scales contribute equally and simultaneously yield log-log plots that are easy to interpret visually, we average $E(k)$ by octaves, that is, a factor of 2 in k,

$$\overline{E_m} = \frac{1}{2^{m-1}} \sum_{j=2^{m-1}}^{2^m-1} E(k_j),\ m = 1, \ldots, \log_2 N - 1\ . \tag{A.11}$$

This corresponds to average wavenumber

$$\overline{k_m} = \frac{1}{2^{m-1}} \sum_{j=2^{m-1}}^{2^m-1} k_j = \frac{3}{2}2^{m-1} - \frac{1}{2},\ m = 1, \ldots, \log_2 N - 1 \tag{A.12}$$

which are equally spaced on a log scale only in the limit $m \gg 1$. We thus obtain exactly $\log_2 N - 1$ estimates for $E(k)$.

A.1.2 Structure Functions

For a stochastic process $\phi(x)$, let us define the absolute increments across scale r,

$$\Delta\phi(r; x) = |\phi(x + r) - \phi(x)|,\ 0 \le r \le L, 0 \le x \le L - r \tag{A.13}$$

and consider their statistical moments. We assume that the statistical properties of $\Delta\phi(r; x)$ are independent of position x. This is weaker than the assumption of stationary increments. Then, because of the scale-invariance, we expect

$$S_q(r) = \langle \Delta\phi(r; x)^q \rangle \equiv \langle \Delta\phi(r)^q \rangle \propto r^{\zeta(q)}\ , \tag{A.14}$$

where $S_q(r)$ is called the structure function of order $q \ge 0$. The family of exponents $\zeta(q)$, as a function of q, has the following properties:

(a) it is normalized,

$$\zeta(0) = 0\ ; \tag{A.15a}$$

(b) it is a convex function (Frisch and Parisi, 1985), i.e.,

$$\zeta''(q) \le 0\ ; \tag{A.15b}$$

(c) finally, if the increments in (A.13) are bounded, $\zeta(q)$ is nondecreasing (Frisch, 1991; Marshak et al., 1994), i.e.

$$\zeta'(q) \geq 0 \; . \tag{A.15c}$$

These last two inequality properties are contingent on the fact that the q-dependence of the prefactors (proportionality constants) in (A.14) is weak enough to neglect.

Two low-order exponents are well known. For $q = 1$, there is

$$0 \leq \zeta(1) = H_1 \leq 1 \; , \tag{A.16}$$

which is called the roughness or Hurst exponent. It characterizes the smoothness of the signal: the larger H_1 the smoother the signal. Referring back to (A.14), the limit $H_1 \to 1$ corresponds to almost everywhere differentiable signals. The opposite limit $H_1 \to 0$ leads to a signal with scale-independent increments. White noise is the most famous example of a signal with $H_1 = 0$, but any scale-invariant stationary process yields the same answer.

The second order ($q = 2$) structure function

$$S_2(r) = \langle |\phi(x + r) - \phi(x)|^2 \rangle \propto r^{\zeta(2)} \tag{A.17}$$

is related to a wavenumber spectrum through the Wiener-Khinchine theorem. This theorem generalized to nonstationary processes with stationary increments (Monin and Yaglom, 1975) reads as

$$1 \leq \beta = \zeta(2) + 1 \leq 3 \; . \tag{A.18}$$

We will use these moments in the examples below.

A.1.3 Examples with Cloud Liquid Water Data

We illustrate the above concepts on cloud liquid water content (LWC) data measured during the Atlantic Stratocumulus Transition Experiment (ASTEX) from an aircraft in June 1992 (Albrecht et al., 1995). Figure A.1a shows a 16384-point data stream sampled approximately every 8 m for an overall length of about 130 km (Davis et al., 1994). So, in the notations of (A.8), we have $N = 2^{14} = 16384$, l = 8 m, and L = 130 km. The wavenumber spectrum of this data set (panel A.1b) follows a power-law behavior (A.2) with spectral exponent $\beta \approx 1.5$ over a quite large range of scales from tens of meters to tens of kilometers. In addition to $N/2 - 1$ wavenumber points, as in (A.10), we also plotted $\log_2 N - 1 = 13$ octave averaged dots as in (A.11)–(A.12). Note that because of fewer contributions from small scales, the octave averaged log-log plot yields slightly smaller spectral exponent ($\beta \approx 1.45$). A detailed discussion of different estimates of spectral exponents for wavenumber spectra can be found in Davis et al. (1996).

The first five integer moments of the absolute increments over scale r, (A.13), for the LWC data in panel A.1a are shown in panel A.1c. Again we see a remarkably

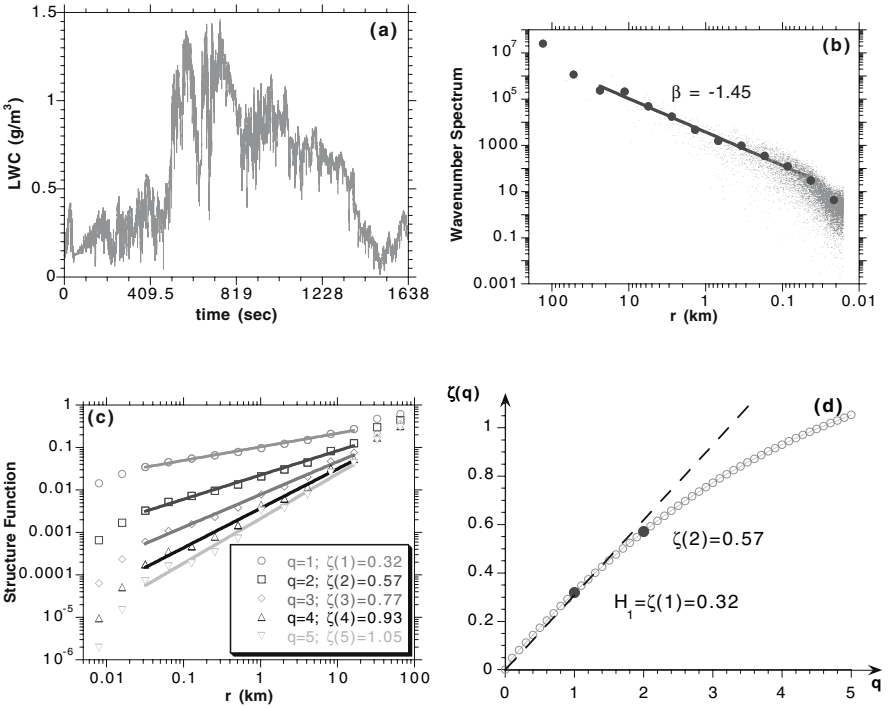

Fig. A.1. Wavenumber spectrum and structure functions of a real-world data set. (**a**) A horizontal transect of cloud liquid water content (LWC) sampled at 10 Hz, 8 m at aircraft speed 80 m/s. The data were collected with the PVM-100 (Gerber, 1991) during the ASTEX experiment in June 1992. (**b**) Wavenumber spectrum for the data on panel (**a**). Circles correspond to the octave-averaged data described in (A.11)–(A.12). (**c**) Structure functions of order 1 to 5 plotted versus scale r. Scaling is indicated from several tens of meters to several tens of kilometers. (**d**) The resulting structure function exponents versus q. The linear relation corresponds to fractional Brownian motion with the same Hurst exponent

good scaling (with correlation coefficient of 0.99) over three orders of magnitude for all five moments. The exponents $\zeta(q)$ of structure function $S_q(r)$ are plotted in panel A.1d. We can easily see that $\zeta(q)$ is a convex nondecreasing function with $\zeta(0) = 0$ as stated in (A.15a)–(A.15c). The Hurst exponent $H_1 = 0.32$ which is typical for marine Sc (Davis et al., 1994, 1999; Marshak et al., 1997). Note that $\zeta(2)+1 = 1.57$ that is close to spectral exponent β in panel A.1b and thus consistent with the Wiener-Khinchine relation in (A.18).

The straight dashed line in panel Fig. A.1d would correspond to fractional Brownian motion (fBm) (Mandelbrot, 1977) with the same Hurst exponent $H = H_1$; i.e.,

$$\zeta(q) = qH \tag{A.19}$$

is a linear function. This linearity is the hallmark of "monoscaling" and, statistically, it corresponds to relatively narrow distributions of the increments across all scales,

e.g., Gaussian distributions which are determined entirely by their variance (and fBm is Gaussian by definition).

The observed nonlinearity or "multiscaling" of $\zeta(q)$ for LWC data indicates a level of intermittency in the data that follows from the non-Gaussian nature of the turbulent signal. Notice that $\zeta(2)$ is visibly lower than the monoscaling prediction $2H_1$. More analysis results and references to data analysis of LWC or other kinds of cloud data can be found, for instance, in Lovejoy and Schertzer (1990), Tessier et al. (1993), Ivanova and Ackerman (1999), and Davis et al. (1999).

A.2 Fractal Models

In this section we describe stochastic models that simulate fluctuations of cloud liquid water. As we saw in the previous section, LWC fluctuations inside marine Sc obey power-law statistics over at least three orders of magnitude in scale. Hence, the main feature we seek in a stochastic model is scale-invariance. In turbulence studies the most popular scale-invariant models are multiplicative cascade models. The construction of a mass-conserving cascade model is as follows (Fig. A.2). Start with a homogeneous slab of length L. Divide into 2 parts and then transfer a fraction f_1 of the mass from one half to the other in a randomly chosen direction. This is equivalent to multiplying the originally uniform density field on either side by factors $W_1^{(\pm)} = 1 \pm f_1$. The same procedure is repeated recursively at ever smaller scales using fractions $f_i (i = 2, 3, \dots)$ on segments of length r_{i+1} where $r_{i+1} = L/2^i$.

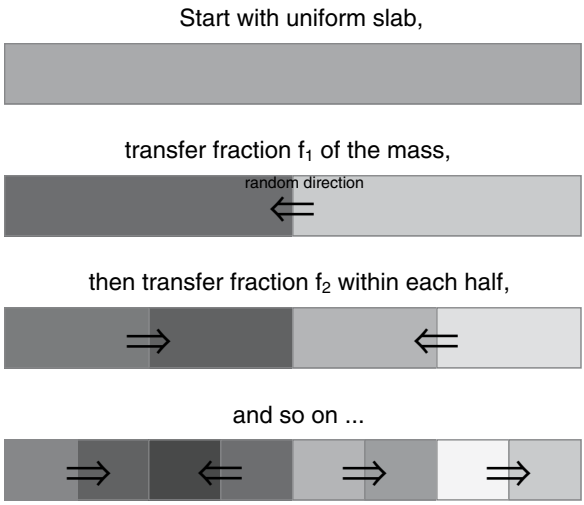

Fig. A.2. Schematic construction of a mass-conservative multiplicative cascade model

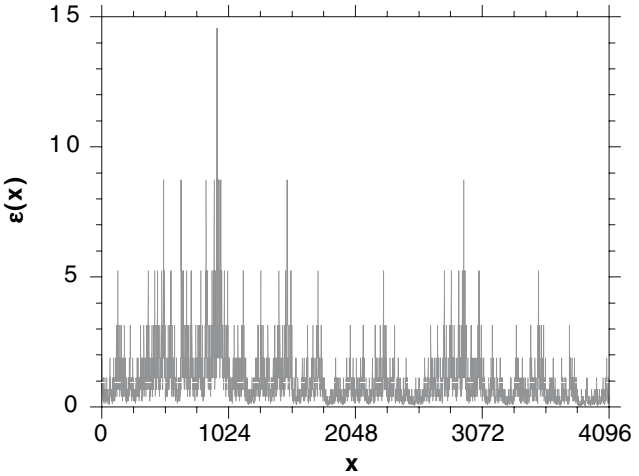

Fig. A.3. A multiplicative 12 cascades "p-model" with unit mean and p = 0.375, thus from (A.21) $\beta_\varepsilon(p) = 0.91$

A.2.1 Singular Cascades

We now parameterize the multiplicative weights as

$$W_i^{(\pm)} = 1 \pm f_i = 1 \pm (1-2p) = \begin{cases} 2p, \text{ or} \\ 2(1-p) \end{cases}, \quad 0 \le p < \frac{1}{2}\,, \tag{A.20}$$

independently of $i = 1, 2, \ldots$, with 50/50 probability for the signs. This leads to a singular (multi)fractal model $\varepsilon(x)$ called the "p-model" (Meneveau and Sreenivasan, 1987); in this model, parameter p controls the degree of mass (energy) redistribution at each cascade step. The p-model (illustrated in Fig. A.3) is scale-invariant; its wavenumber spectrum exhibits a power law, $E_\varepsilon(k) \propto k^{-\beta_\varepsilon}, k > 0$, with spectral exponent

$$0 \le \beta_\varepsilon(p) = 1 - \log_2[1 + (1-2p)^2] < 1\,. \tag{A.21}$$

Singular cascade models $\varepsilon(x)$ have interesting intermittency properties but their spectra with $\beta_\varepsilon < 1$ do not scale as observed cloud liquid water fields (that have $\beta > 1$) and therefore they do not show stochastic continuity.

A.2.2 Bounded Cascades

A simple way to obtain $\beta > 1$ is to reduce the variance of the multiplicative weights in (A.20) at each cascade step. Taking

$$W_i^{(\pm)} = 1 \pm (1-2p)2^{-H(i-1)}, 0 \le p < 1/2, H > 0, i = 1, 2, \ldots \tag{A.22}$$

leads to "bounded" cascade models (Cahalan, 1994). The limit $H \to \infty$ yields a single jump (Heaviside step) from $2p$ to $2(1-p)$ at $x = L/2$.

By reducing the size of the jumps as the scale decreases, we are effectively introducing a degree of continuity into the model. One can show that in this case, its autocorrelation function is a continuous function at $r = 0$ and a generated field $\phi(x)$ is stochastically continuous (A.7). As a result, the spectral exponent has moved into the range

$$1 < \beta_\phi(H) = \min\{2H, 1\} + 1 \leq 2 \,, \tag{A.23}$$

independently of p. Figure A.4 (top panel) shows a realization of a 14-step bounded cascade model with $H = 1/3$ and $p = 0.375$.

In the limit of an infinite number of cascade-steps, the structure function exponents $\zeta(q)$ have a nonlinear form (Marshak et al., 1994),

$$\zeta(q) = \min\{qH, 1\} = \begin{cases} qH, & 0 \leq q \leq 1/H \\ 1, & 1/H \leq q < \infty \end{cases} \,; \tag{A.24}$$

so (A.23) follows from (A.18) and (A.24). Since the spectral exponents of a monoscaling fBm is a linear function, $\zeta(q) = qH$, the bounded cascade model cannot be distinguished from fBm for moments smaller than $q = 1/H$. This is clearly seen in Fig. A.5 which shows theoretical structure function exponents for both bounded models (A.24) and fBm (A.19).

To summarize, the bounded cascade model is a good tutorial model for cloud horizontal inhomogeneity. To a first approximation, it reproduces lower-order statistical moments of cloud liquid water distribution. However, as follows from (A.24), its $\zeta(q) = 1$ for $q \geq 1/H$ whereas the higher-order moments of LWC fluctuations have exponents that substantially exceed unity and show strong curvature even for low values of q. In the next subsection we describe another model, fractionally integrated cascades (Schertzer and Lovejoy, 1987) that overcomes these limitations.

A.2.3 Fractional Integration

Another way of transforming singular cascades with $\beta_\varepsilon < 1$ into a more realistic one with $\beta_\phi > 1$ is power-law filtering in Fourier space (Schertzer and Lovejoy, 1987); this will bring the spectral exponent to any prescribed value. In particular, we have

$$\beta_\phi(p, H^*) = \beta_\varepsilon(p) + 2H^* \tag{A.25}$$

where $0 < H^* < 1$ describes the low-pass filter in k^{-H^*}. Mathematically, this operation – also known as "fractional integration" (FI) – is a convolution with a weakly singular kernel:

$$\phi(x) = \int \varepsilon(y)|x - y|^{H^*-1}\mathrm{d}y \,. \tag{A.26}$$

This is called FI since for $H^* = 1$ it corresponds to ordinary integration. Here again, thanks to the FI term in (A.25), field $\phi(x)$ is stochastically continuous. As an example, Fig. A.4 shows a realization of the FI cascade model with $p = 0.375$ (thus

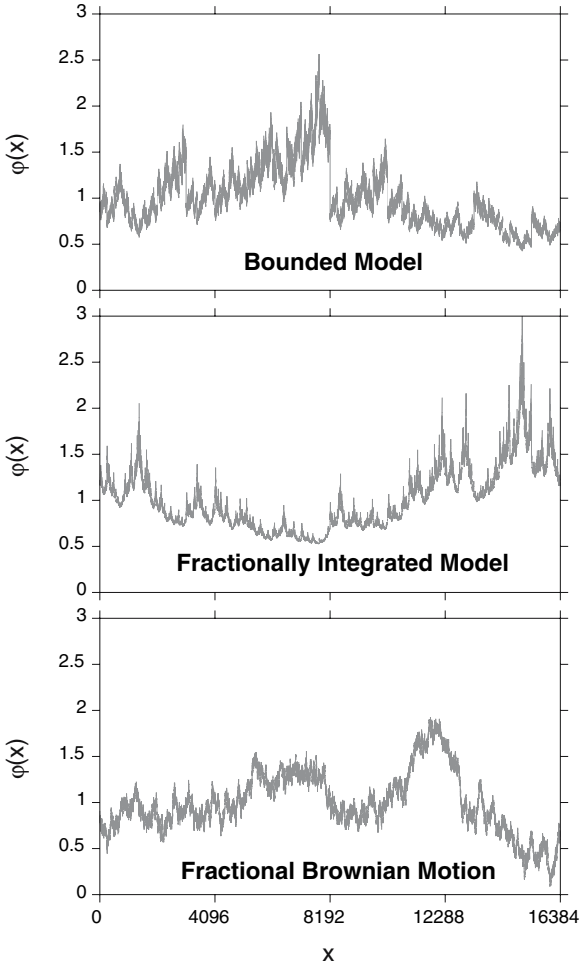

Fig. A.4. Three fractal models with the same spectral exponent $-5/3$ and overall mean and variance. From *top* to *bottom*: bounded (Bo) cascade model with $H = 1/3$ and $p = 0.375$; fractionally integrated (FI) cascade model with $p = 0.375$ and $H^* = 0.38$; fractional Brownian motion (fBm) with $H = 1/3$. Bo and FI are generated with 14 cascade steps; fBm is generated using mid-point displacement method (e.g., Peitgen and Saupe, 1988) also with 14 steps. As a result, all models have $2^{14} = 16384$ pixels. In all three models average $\langle\phi\rangle = 1$ and standard deviation $= 1/3$. Note that, by construction, both Bo and FI multiplicative cascade models have only positive values while $\phi(x)$ for fBm can be either positive or negative since its probability density function is Gaussian

$\beta_\varepsilon(p) = 0.91$) and $H^* = 0.38$ (thus $\beta_\phi(p, H^*) = 5/3$). In contrast to the bounded model, we have only approximate formulas for the structure function exponents for FI model. They are exact for $q = 0$ and $q = 2$ and quite accurate for all low-order moments and, moreover, numerical results are always available.

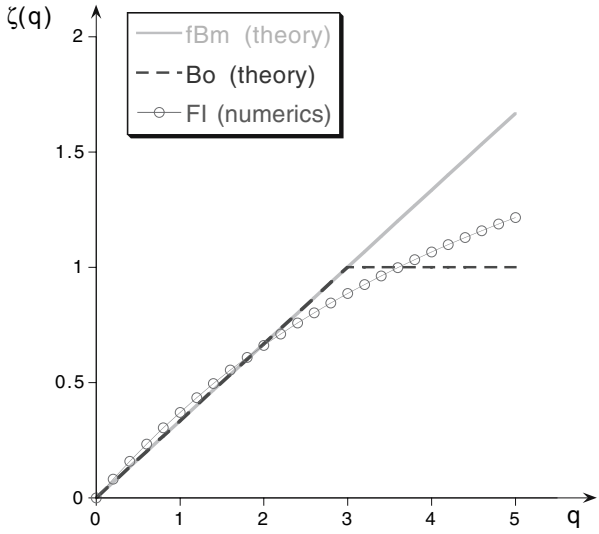

Fig. A.5. Comparison of exponent functions $\zeta(q)$ for three fractal models. Fractional Brownian motion (fBm) with $H = 1/3$, bounded cascades (Bo) with $H = 1/3$ and fractionally integrated (FI) cascades with $p = 0.375$ and $H^* = 0.38$. Note that while for fBm and Bo models we give theoretical curves, FI shows the results of numerical calculations with 15 cascade steps averaged over 100 realizations

To compare the three models (monoscaling fBm and two multiscaling models, bounded and FI cascades), we plotted their structure function exponents $\zeta(q)$ in Fig. A.5 for q going from 0 to 5. As we see, the bounded model is the most intermittent among them since its $\zeta(q)$ is the most nonlinear. However, with at least one more tunable parameter than bounded cascades, FI cascades are better candidates for simulating observed liquid water fluctuations.

References

Albrecht, B.A., C.S. Bretherton, D. Johnson, W.H. Schubert, and A.S. Frisch (1995). The Atlantic Stratocumulus Transition Experiment – ASTEX. *Bull. Amer. Meteor. Soc.*, **76**, 889–904.

Cahalan, R.F. (1994). Bounded cascade clouds: Albedo and effective thickness. *Nonlinear Proc. Geophys.*, **1**, 156–167.

Davis, A., A. Marshak, W.J. Wiscombe, and R.F. Cahalan (1994). Multifractal characterizations of nonstationarity and intermittency in geophysical fields: Observed, retrieved, or simulated. *J. Geophys. Res.*, **99**, 8055–8072.

Davis, A., A. Marshak, W.J. Wiscombe, and R.F. Cahalan (1996). Scale-invariance in liquid water distributions in marine stratocumulus, Part I, Spectral properties and stationarity issues. *J. Atmos. Sci.*, **53**, 1538–1558.

Davis, A.B., A. Marshak, H. Gerber, and W.J. Wiscombe (1999). Horizontal structure of marine boundary-layer clouds from cm- to km-scales. *J. Geophys. Res.*, **104**, 6123–6144.

Frisch, U. (1991). From global scaling, à la Kolmogorov, to local multifractal scaling in fully developed turbulence. *Proc. Roy. Soc. London. A*, **434**, 89–99.

Frisch, U. and G. Parisi (1985). A multifractal model of intermittency. In *Turbulence and Predictability in Geophysical Fluid Dynamics*. M. Ghil, R. Benzi and G. Parisi (eds.). North Holland, Amsterdam, The Netherlands, pp. 84–88.

Gerber, H. (1991). Direct measurement of suspended particulate volume concentration and far-infrared extinction coefficient with a laser-diffraction instrument. *Atmos. Res.*, **30**, 4824–4831.

Ivanova, K. and T.P. Ackerman (1999). Multifractal characterization of liquid water in clouds. *Phys. Rev. E*, **59**, 2778–2782.

Lovejoy, S. and D. Schertzer (1990). Multifractals, universality classes and satellite and radar measurements of cloud and rain fields. *J. Geophys. Res.*, **95**, 2021–2034.

Mandelbrot, B.B. (1977). *Fractals: Form, Chance, and Dimension*. W.H. Freeman, San Francisco (CA).

Marshak, A., A. Davis, R.F. Cahalan, and W.J. Wiscombe (1994). Bounded cascade models as non-stationary multifractals. *Phys. Rev. E*, **49**, 55–69.

Marshak, A., A. Davis, W.J. Wiscombe, and R.F. Cahalan (1997). Scale-invariance of liquid water distributions in marine stratocumulus, Part 2 – Multifractal properties and intermittency issues. *J. Atmos. Sci.*, **54**, 1423–1444.

Meneveau, C. and K.R. Sreenivasan (1987). Simple multifractal cascade model for fully developed turbulence. *Phys. Rev. Lett.*, **59**, 1424–1427.

Monin, A.S. and A.M. Yaglom (1975). *Statistical Fluid Mechanics*, volume 2. MIT Press, Boston (MA).

Papoulis, A. (1965). *Probability, Random Variables, and Stochastic Processes*. McGraw-Hill, New York (NY).

Peitgen, H.-O. and D. Saupe (1988). *The Science of Fractal Images*. Springer-Verlag, New York (NY).

Schertzer, D. and S. Lovejoy (1987). Physical modeling and analysis of rain and clouds by anisotropic scaling multiplicative processes. *J. Geophys. Res.*, **92**, 9693–9714.

Tessier, Y., S. Lovejoy, and D. Schertzer (1993). Universal multifractals: Theory and observations for rain and clouds. *J. Appl. Meteor.*, **32**, 223–250.

Epilogue: What Happens Next?

Radiative Transfer Problems

Let's make the circumstantially reasonable assumption that we have a tough radiative transfer (RT) problem to solve. Maybe clouds are in the picture. For simplicity, let's assume it is a "forward" RT problem where we know the optical properties of the atmosphere and surface. If we are faced with an "inverse" problem, as is often the case in remote sensing, then we first need to establish that we can solve the forward problem anyway. We are thus asked to compute some radiance values $I(\boldsymbol{x}, \boldsymbol{\Omega})$ for a given wavelength where $\boldsymbol{x}$ is position in three-dimensional (3D) space and $\boldsymbol{\Omega}$ is a direction of propagation on the unit sphere.

In remote sensing, $\boldsymbol{x}$ is likely to be the position of a sensor and $-\boldsymbol{\Omega}$ will be the direction it is looking into, defined (say) by one of many pixels at the focal plane.[1] In radiation energy budget modeling, we are only interested in angular integrals of $I(\boldsymbol{x}, \boldsymbol{\Omega})$, weighted or not with $|\Omega_z|$ (the vertical direction cosine). At any rate, we now have to somehow find a solution of the integro-differential RT equation that looks like

$$\boldsymbol{\Omega} \bullet \nabla I = -\sigma(\boldsymbol{x})[I(\boldsymbol{x}, \boldsymbol{\Omega}) - \varpi_0 \int_{4\pi} p(\boldsymbol{\Omega}' \bullet \boldsymbol{\Omega}) I(\boldsymbol{x}, \boldsymbol{\Omega}') \mathrm{d}\boldsymbol{\Omega}'] + Q(\boldsymbol{x}, \boldsymbol{\Omega})$$

in the relatively simple case where scattering properties, single-scattering albedo ϖ_0 and phase function p, are assumed uniform but the extinction coefficient $\sigma(\boldsymbol{x})$ varies spatially. $Q(\boldsymbol{x}, \boldsymbol{\Omega})$ is a given volume source term, e.g., thermal emission. There will also be boundary conditions to satisfy and, for simplicity, we will assume these boundaries are flat, at a constant z-coordinate: the upper (top-of-atmosphere, TOA) condition is typically an incoming uniform collimated solar beam; the lower (surface) condition can be quite complex, with spatially and angularly varying reflection and/or emission. If there is an interest in polarization, then I is a 4-vector and p is a

[1] From large stand-off distances, $\boldsymbol{x}$ can also be viewed as a variable point on the upper boundary of the atmosphere-surface medium and $\boldsymbol{\Omega}$ is then the constant (or $\boldsymbol{x}$-dependent, depending on distance) direction of the sensor.

4×4 matrix – a relatively minor complication in view of all the spatial and angular variables in the balance.

The above stated 3D RT problem includes the majority of current remote sensing and climate needs. But we still have to find a way to solve the scalar or vector RT equation.

Classic Solutions, and Their Limitations

There are only two situations where exact solutions exist, clearly a desirable scenario and especially in remote sensing:

1. $\varpi_0 = 0$ (no scattering) and a non-reflecting surface, hence no coupling at all between beams in direction or in polarization. In this case, $\sigma(\boldsymbol{x})$ and $Q(\boldsymbol{x}, \boldsymbol{\Omega})$ can be arbitrarily complicated, and the same is true for the surface source distribution. Here, we can even write an analytical expression for $I(\boldsymbol{x}, \boldsymbol{\Omega})$: a one-dimensional integral along the beam $\{\boldsymbol{x}, \boldsymbol{\Omega}\}$ using the boundary source, Q, and transmission functions (negative exponentials of line-integrals of σ under the present monochromatic assumption).
2. $\sigma(\boldsymbol{x}) \equiv \sigma(z)$ and $Q(\boldsymbol{x}, \boldsymbol{\Omega}) \equiv Q(z, \boldsymbol{\Omega})$, hence $I(\boldsymbol{x}, \boldsymbol{\Omega}) \equiv I(z, \boldsymbol{\Omega})$. This is the famous horizontally uniform atmosphere/surface plane-parallel system of one-dimensional (1D) RT. Under the present assumptions of vertically uniform scattering properties, $0 < \varpi_0 \leq 1$ and $p(\cdot)$, this multiple-scattering problem is amenable, via invariant embedding and superposition, to Chandrasekhar's H-, or X- and Y-functions using the dimensionless coordinate $\mathrm{d}\tau = \sigma(z)\mathrm{d}z$.

If, in problem #1, the surface becomes partially reflective then there will be at the most one reflection off the (flat) ground. Thus, if a surface point $\boldsymbol{x}_S$ is in view, an angular integral over the down-welling hemisphere (weighted by surface reflectivity and $|\Omega_z|$) of the closed-form solutions at $\boldsymbol{x}_S$ is required to adjust the boundary source term. Then the exact 1D solution along the beam going from the sensor to $\boldsymbol{x}_S$ can be applied. Early releases of the remote-sensing workhorse code known as MODTRAN were designed specifically to solve this problem for a 1D (i.e., stratified) atmosphere.[2] If, in problem #2, the scattering properties ϖ_0 and p become dependent on the sole spatial coordinate $\tau(z)$ of the 1D RT problem, then we know how to obtain accurate numerical solutions using popular codes such as DISORT or, for spectral details, a recent release of MODTRAN (which will in fact call DISORT for the multiple scattering).

[2] The main problem that MODTRAN designers, and contributing molecular spectroscopy experts, address is the weighted (sensor-response) integration over potentially complicated and fast spectral variability of absorbing atmospheric gases computed on the fly for a given atmospheric composition. The MODTRAN solution to the spectral variability problem generally requires averaging over many values of the extinction/absorption coefficient σ, even at the smallest allowable wavelength interval. This spectral averaging in turn leads to transmission functions that are not exponential in the amounts of absorbers. MODTRAN developers have also enabled spherical 1D (stratified) geometry, including refractivity.

That's it. Every other solution of the 3D RT equation will call for some sophisticated mathematical analysis, an intricate time-consuming numerical implementation, and then probably too many computer cycles . . . so only research-mode utilization is contemplated. At least that is the conventional wisdom. It is therefore not surprising that virtually all operational remote sensing and radiation energy budget estimations are done with one of the above pair of text-book solutions, too often regardless of their applicability.

Take, for instance, atmospheric sounding – extracting (say) temperature and water vapor profiles, via $\sigma(z)$ and $Q(z)$, from measured I(ground, zenith) or I(TOA, nadir) at a number of wavelengths. This application uses the "no-scattering" solution #1, often in the microwave region where its strong assumptions are considered reasonably valid. But are they really? Apparently not in the presence of heavy precipitation.

In radiation energy budget problems, two "streams" of radiation (one up and one down) are usually considered sufficient. Schuster, arguably the founding father of atmospheric RT, showed – one hundred years ago at the time of writing – that the "scattering/absorption" problem #2 then becomes analytically tractable in closed-form. This outcome is always a plus in applications such as GCM-based climate simulations where very many RT computations need to be performed (one per layer and per cell and at as many time-steps as possible). But can we be confident in century-old transport physics for such a critical aspect of the the climate problem?

A New Perspective on Atmospheric Radiative Transfer

The above formulation of 3D RT in the atmosphere/surface system is not just a challenging problem in computational physics. It should be viewed as an accurate description of the photon flow that is actually unfolding in Nature. It is a codified representation of the reality we are dealing with, hardly a "problem." So the preferred *mathematically exact* solutions #1 and #2 are in fact just *physical approximations*. Indeed, a purely emitting/absorbing medium is an abstraction . . . as we know from practical thermodynamics that it is impossible to make a perfect black-body (every material will reflect or scatter at least a little).[3] And of course, an exactly uniform plane-parallel cloud layer has never materialized since cloud structure and evolution are part of normal tropospheric dynamics. These fluid dynamics (a.k.a. "weather") are clearly stratified (lapse rates, boundary layers, inversion layers, etc.) but they are also very 3D in nature at all scales (general circulation, fronts, waves, jets, convection, precipitation, instability, turbulence, and so on).

We can make an immediate damage assessment here. Any volume scattering perturbs solution #1 and horizontal gradients in anything perturb solution #2 for scattering media. In cloud remote sensing at optical wavelengths, blind faith in solution #2 is to believe that satellite pixels are radiatively independent. That would be reasonable only if they were huge. But then again, if we approximated that situation by

[3] For the more theoretically minded, this is traceable to the Kramers-Kronig causality relations, a precursor to the linear response formalism for transport coefficient estimation.

aggregating enough pixels deemed too-small, would it be reasonable to assume the pixels are internally uniform?

Much of the 3D RT literature so far has used the uniform plane-parallel cloud model as a benchmark, estimating the bias associated with that 1D model simply because it is so widely accepted. We propose that for the next century of atmospheric RT, the plane-parallel model be considered what it really is: an approximation that, like any other, needs validation or at least a convincing justification. It should not be a convenient assumption we can make . . . just because most everyone else does, just because that is what MODTRAN delivers.

For instance, letting $\boldsymbol{\Omega} = (\sin\theta\cos\phi, \sin\theta\sin\phi, \cos\theta)^{\mathrm{T}}$ in the usual polar representation and looking back at the *left-hand side* of the above 3D RT equation, a modeler intent on using 1D RT should explain to the end-user why

$$\sin\theta \left| \cos\phi \frac{\partial I}{\partial x} + \sin\phi \frac{\partial I}{\partial y} \right| \ll \left| \cos\theta \frac{\partial I}{\partial z} \right| \ .$$

This case for weak "3D-ness" can be made by stating the (preferably low) value of ϖ_0 and/or by noting that $\sigma(\boldsymbol{x})$ is a stronger function of z than of $\vec{x} = (x, y)^{\mathrm{T}}$, by making a solid theoretical argument based on a conceptual model, by using a computational 3D model as a benchmark, by analyzing real-world data which is 3D-compliant by definition, or any combination of these approaches. At least this way we collectively reinforce the awareness that 1D RT is an approximate solution of the real 3D RT problem at hand.

Assuming the case for using a 1D model has been made, what will be done with the residual horizontal variability ($\vec{x}$-dependence) of $\sigma(\boldsymbol{x})$ and $Q(\boldsymbol{x}, \boldsymbol{\Omega})$ on the *right-hand side* of the transport equation? Will it be averaged out? Will it be treated parameterically? That is, extinction in the 1D transport solver will be processed as $\sigma(z; \vec{x})$ where the semi-colon emphasizes the difference between variables and parameters. This is known as the local Independent Column Approximation (ICA). Will we horizontally average the outcome of the local ICA result, say, for I(TOA,nadir), over all $\vec{x}$ values? Will an "effective" extinction be used that attempts to capture 3D effects in some statistical sense? And what will we do about $Q(\boldsymbol{x}, \boldsymbol{\Omega})$? At any rate, we can no longer say: *What else than 1D RT can be done?* This monograph demonstrates that much more can be done, and not necessarily at a large computational cost.

The above questions collide head-on with a new and interesting quantity that arises in 3D RT modeling. What is the "scale" r of interest? & What are the RT "dynamics" of $\overline{I}_r(\boldsymbol{x}, \boldsymbol{\Omega})$, the radiance field coarse-grained to scale r? The instinctive answer will likely be that r is the resolution of the instrument (the pixel-size) or the mesh spacing in the climate- or cloud-dynamics model (the grid-constant). These are important but *artificial scales*. First, sensors as well as computational meshes are becoming ever-more "adaptive," so pixel- or grid-scales are moving targets. Second, there are equally if not more important *physical scales* and dimensionless ratios thereof to consider: the photon mean-free-path, the cloud-layer thickness, the photon diffusion scale, cloud aspect ratio, dominant variability scales, and so on.

Where observational or computational resolution plays an essential role, at least from the 3D RT modeling perspective, is in telling us whether or not the variability of concern is resolved. What comes next?

- In the case of resolved variability, we have to worry about (the divergence of net) radiative fluxes that cross boundaries of pixels or grid-cells. These fluxes will invalidate a preemptive 1D treatment of the RT. Is there a simple way to estimate them and remove the bias from the 1D model?
- In the case of unresolved variability, we have to make statistical assumptions about it and try to estimate its likely impact on the resolved scales. Can we formulate an "effective medium" theory where modified optical properties will incorporate the bulk effects of small-scale fluctuations?

In 3D reality of course, both processes are at work to some extent. At any rate, we must learn how to manage all the identified radiative processes at various scales and make informed decisions about their importance based on experience and on programmatic priorities. This is by no means easy. All too frequently, the "ignorance is bliss" modus-operandi prevails.

Time: The New Frontier in Atmospheric Remote Sensing

Time-dependence is a dimension of RT that we have only started to explore in any depth for real – that is, 3D – atmospheric RT. So now we consider $I(t, \boldsymbol{x}, \boldsymbol{\Omega})$, typically with $t \geq 0$, that obeys a RT equation in "$3 + 1$" dimensions: the volume- and/or boundary-sources become t-dependent and, most notably, the monokinetic advection operator $\boldsymbol{\Omega} \bullet \nabla$ becomes[4]

$$\frac{1}{c}\frac{\partial}{\partial t} + \boldsymbol{\Omega} \bullet \nabla \ .$$

Even for steady-state photon transport in 1D geometry, the dominant number of scattering events or mean photon time-of-flight for a given outcome (e.g., reflection versus transmission) are profoundly informative quantities. There is already a core international community invested in differential absorption spectroscopy in the oxygen A-band as a means of accessing solar photon path length statistics. These new observables have proven to be highly sensitive to the degree of spatial complexity in cloudiness, e.g., single/unbroken layers versus multiple and/or broken layers. Pulsed (laser) sources or rapidly time-varying sources (e.g., lightning flashes) can be traced along convoluted multiple-scattering paths through dense clouds. Thanks to recent technological advances, we can now observe the resulting waveforms, and these can be analyzed in terms of cloud or source properties using time-dependent RT, in 3D as needed.

[4] Somewhat miraculously, this is not so new as it appears at first glance, at least for pulsed sources. A temporal Laplace transform indeed converts the t-derivative into what looks like a spatially uniform (hence gaseous) absorption term with a coefficient varying from 0 to ∞ while the δ-in-time source term becomes a constant. The converse statement – if we know the detailed t-dependence, then we can compute the effect of any level of gaseous absorption – is known as the "Equivalence Theorem."

Last but not least, temporal (i.e., pulse-stretching) scales and some of the above-mentioned spatial scales are so tightly connected through the fractal nature of photon random walks in the Earth's cloudy atmosphere that they are really just two sides of the same coin. This insight has far-reaching ramifications that, in particular, have yet to be exploited for the teaching of radiative transfer through geometry and probability rather than through calculus.

In summary, we feel that future generations of atmospheric and remote-sensing scientists, whether or not they become "RT" experts, need to be exposed to the rich phenomenology of 3D radiative transfer and encouraged to explore it to their young heart's content.

Los Alamos, New Mexico *Anthony Davis*
January, 2005 *Alexander Marshak*

Notations

In this volume, we have adopted standard notations for radiance/intensity $I_\lambda(\boldsymbol{x}, \boldsymbol{\Omega})$, irradiance/flux $F_\lambda(\boldsymbol{x})$, transmittance T, optical depth τ, extinction σ, and so on, from the astrophysical and transport-theoretical literatures because they are also very well known in the geophysics community. However, some readers more familiar with remote-sensing textbooks will recognize respectively L_λ, E_λ, τ, δ, β, etc.

Square brackets designate an [alternate] name or unit for some quantity. Parentheses identify an (optional qualifier) of some quantity's name, or units that can be omitted by proper normalization and/or spectral integration. A dagger† designates a quantity that can be "spectral," and therefore carry a subscript λ or ν as in Planck function; in this case, (/μm) or (/cm^{-1}) appears in their units. In solar problems, where one can set $\mu_0 F_0$ to unity, these quantities can be non-dimensionalized altogether (hence the optional units of W/m^2). Many other optical quantities, e.g., σ or τ, can depend *parameterically* on λ or ν but this does not affect their units.

1 Scalar and Vector Quantities, about Units

In the following table, four different SI-derived units of length are used – sometimes in combinations – and each has its dedicated purpose in accounting for cloud optics, microphysics, radiation sources/sinks and transport:

- the "μm" is assigned to wavelengths and particle sizes (hence to spectral and/or single-scattering considerations in cloud/aerosol optics);
- the "cm" is assigned to droplet densities (hence to cloud microphysical considerations);
- the "m" is assigned to flux/irradiance units (hence to radiation budget considerations);
- the "km" is assigned to photon transport coefficients and scales of variability in clouds, including outer scales such as physical thickness (hence to all radiative transfer considerations).

In the volume, yet another derived SI unit is used occasionally, following established tradition: the "mm," for vertically-integrated liquid- and/or ice-water in cloud layers, while the "cm" is often used for total precipitable water in the atmosphere (always dominated by the vapor phase).

1. SCALAR AND VECTOR QUANTITIES, BEGIN

Symbol	Name	Relation to Others	Units (-: none)
A	absorptance		–
A_c	cloud fraction		–
$B_\nu(T)$	Planck('s) function	$2h\nu^3/c^2(\mathrm{e}^{h\nu/kT}-1)$	W/m^2/cm^{-1}/sr
$B_\lambda(T)$	Planck('s) function, by wavelength	$B_{\nu(\lambda)}(T)\,\lvert d\nu/d\lambda\rvert(\lambda)$	W/m^2/μm/sr
BRF	(boundary) radiance as a Bidirectional Reflection Function	$\pi I/\mu_0 F_0$	–
d	distance		km
D	(radiative [photon]) diffusivity	$c\ell_\mathrm{t}/3$	km^2/s
D'	diffusivity, for steady-state	$D/c=\ell_\mathrm{t}/3$	km
$\boldsymbol{F}$	(radiant energy) flux vector†	$\int \boldsymbol{\Omega} I(\cdot,\boldsymbol{\Omega})\mathrm{d}\boldsymbol{\Omega}$	(W/m^2(/μm))
$\boldsymbol{F}'$	photon flux [current density] vector†	$\boldsymbol{F}/h\nu$	(m^{-2}s^{-1}(μm^{-1}))
F_u, $F_\uparrow$	upward (hemispherical) flux [irradiance]†	$\int_{\mu>0}\mu I(\cdot,\boldsymbol{\Omega})\mathrm{d}\boldsymbol{\Omega}$	(W/m^2(/μm))
F_d, $F_\downarrow$	downward (hemispherical) flux [irradiance]†	$\int_{\mu<0}\lvert\mu\rvert I(\cdot,\boldsymbol{\Omega})\mathrm{d}\boldsymbol{\Omega}$	(W/m^2(/μm))
F_0, $F_\odot$	solar constant [flux] [irradiance]†		(W/m^2(/μm))
g	asymmetry factor (of phase function)	$2\pi\int \mu_\mathrm{s} P(\mu_\mathrm{s})\mathrm{d}\mu_\mathrm{s}$	–
h	cloud geometrical [physical] thickness		km
H	(vertical integral of) horizonal flux (divergence)	$1-(A+R+T)$	–
$I(\boldsymbol{x},\boldsymbol{\Omega})$	radiance [(specific) intensity]†		(W/m^2(/μm))/sr
$I_0(\boldsymbol{x})$	directly transmitted [un-collided] radiance†		(W/m^2(/μm))/sr
J	scalar [spherical, or actinic] flux†	$\int I(\cdot,\boldsymbol{\Omega})\mathrm{d}\boldsymbol{\Omega}$	(W/m^2(/μm))
J'	scalar [spherical, or actinic] photon flux†	$J/h\nu$	(m^{-2}s^{-1}(μm^{-1}))
k	wavenumber [Fourier-conjugate of position]	$(2\pi\times)1/r$	(rad)km^{-1}
k, k_ν, k_λ	(gaseous) absorption coefficient		km^{-1}
K, $\mathcal{K}$	kernel of an integral RT equation		km^{-3}sr^{-1}

1. SCALAR AND VECTOR QUANTITIES, CONTINUED

Symbol	Name	Relation to Others	Units (-: none)
$L, \mathcal{L}$	integro-differential operator in RT equation		km^{-1}
L	(cumulative [total]) (geometrical) (photon) path((-)length)	ct	km
L_d	diffusion length	$\ell/\sqrt{3(1-\varpi_0)(1-\varpi_0 g)}$	km
L_D	horizontal domain size [outer scale]		km
$\mathcal{L}, L_\mathrm{wc}$	liquid water content		$\mathrm{g/m}^3$
ℓ	(local) (photon) mean-free-path, or "MFP"	$1/\sigma$	km
ℓ_t	transport mean-free-path	$\ell/(1-\varpi_0 g)$	km
n	order [number] of scattering[s]		–
$n(r)$	(cloud) droplet [particle] size-distribution [-spectrum]		$\mathrm{cm}^{-3}/\mu\mathrm{m}$
N	(cloud) droplet [particle] density	$\int n(r)\mathrm{d}r$	cm^{-3}
$p(\mathbf{\Omega} \rightarrow \mathbf{\Omega}')$	(scattering) phase function	$\int_{4\pi} p(\mathbf{\Omega} \rightarrow \mathbf{\Omega}')\mathrm{d}\mathbf{\Omega} = 1$	1/sr
$p(\cos\theta_\mathrm{s})$	(azimuthally-symmetric) phase function	$2\pi\int_{-1}^{+1} p(\cos\theta_\mathrm{s})\mathrm{d}\cos\theta_\mathrm{s} = 1$	1/sr
$P(\theta_\mathrm{s})$	(alternately normalized) phase function	$\int_{-\pi}^{+\pi} P(\theta_\mathrm{s})\sin\theta_\mathrm{s}\mathrm{d}\theta_\mathrm{s} = 2$	–
$Q(\boldsymbol{x}, \mathbf{\Omega})$	source term† in RT equation		$(\mathrm{W/m}^2/\mu\mathrm{m}))/\mathrm{sr/km}$
r	distance [scale (in spatial statistics)]	$[(2\pi\times)1/k]$	km
r	droplet [particle] radius		μm
$\langle r^q \rangle$	qth moment of droplet [particle] radius	$\int r^q n(r)\mathrm{d}r/N$	$\mu\mathrm{m}^q$
r_e	effective (droplet) radius	$\langle r^3\rangle/\langle r^2\rangle$	μm
R	reflectance [albedo]		–
s	cross-section (per particle)		m^2
s	(photon) free path [step] (between two collisions)		m
s	Laplace-conjugate (variable) of time t		s^{-1}
S	similarity factor	$\ell_\mathrm{t}/L_\mathrm{d}$	–
$S(\boldsymbol{x}, \mathbf{\Omega})$	source function†	$\sigma_\mathrm{s}(\boldsymbol{x})\int p(\mathbf{\Omega}' \rightarrow \mathbf{\Omega}) I(\boldsymbol{x}, \mathbf{\Omega}')\mathrm{d}\mathbf{\Omega}'$	$(\mathrm{W/m}^2/\mu\mathrm{m}))/\mathrm{sr/km}$
t	time		s

1. SCALAR AND VECTOR QUANTITIES, CONTINUED

Symbol	Name	Relation to Others	Units (-: none)
T	temperature		K [°C]
T	(total) transmittance	$T_{0[\mathrm{dir}]} + T_{\mathrm{d(if)}}$	–
$T_0, T_{\mathrm{dir}}, \mathcal{T}$	direct [un-collided] transmittance		–
$T_{\mathrm{d}}, T_{\mathrm{dif}}$	diffuse transmittance		–
U	photon [radiant energy] density	J/c	m^{-3} [$\mathrm{J/m}^3$]
W	liquid water path	$\int \mathcal{L} \mathrm{d}z$	$\mathrm{g/m}^2$
W'	liquid water path	W/ρ_{w}	cm [mm]
x, y, z	(Cartesian) coordinates, with z increasing upwards		km
$\boldsymbol{x}$	position (in 3D space)	$(x, y, z)^{\mathrm{T}}$	km
$\vec{x}$	position in the horizontal plane	$(x, y)^{\mathrm{T}}$	km
$\boldsymbol{x}_{\mathrm{S}}$	position on the 2D boundary of a 3D volume		km
α	(planar) albedo		–
α_{S}	surface albedo		–
χ	(numerical) extrapolation length factor	$O(1)$	–
$\chi\ell_{\mathrm{t}}$	extrapolation length		km
ε	emissivity		–
λ	wavelength	$10^4[c]/\nu$	µm [m]
λ	(dimensionless) optical pathlength [cumulated extinction]	σL	–
μ	cosine of zenith [polar] angle	$\cos\theta$	–
$\mu_0 > 0$	cosine of solar (zenith) angle	$\cos\theta_0$	–
μ_{s}	cosine of scattering angle	$\cos\theta_{\mathrm{s}}$	–
ν	frequency [wavenumber] (of photon [E-M wave])	$10^4[c]/\lambda$	cm^{-1} [Hz]

1. SCALAR AND VECTOR QUANTITIES, END

Symbol	Name	Relation to Others	Units (-: none)
ϕ	azimuthal angle		°[rad]
ϕ_0	solar azimuthal angle		°[rad]
ϕ_s	scattering azimuthal angle		°[rad]
ϖ_0	single-scattering albedo	σ_s/σ	–
ρ	horizontal radius [displacement]	$\sqrt{x^2+y^2}$	km
ρ	(ground) reflectivity [albedo]		–
ρ, n, N	(particle [mass]) density		m^{-3} (kg/m^3)
σ, σ_e	extinction (coefficient)	$\sigma_a + \sigma_s$	km^{-1}
σ_a	absorption coefficient	$s_a N$	km^{-1}
σ_s	scattering coefficient	$s_s N$	km^{-1}
τ	optical distance	$\int \sigma ds]$	–
τ, τ_c	(cloud) optical depth [thickness]	$h/\ell = \sigma h$	–
τ_t	transport [rescaled] optical depth [thickness]	$h/\ell_t = (1-\varpi_0 g)\tau$	–
θ	zenith [polar] angle, with $\theta = 0$ meaning "up"		°[rad]
$\theta_0 < \pi/2$	solar (zenith) [incidence] angle		°[rad]
θ_s	scattering angle	$\cos^{-1}(\boldsymbol{\Omega} \bullet \boldsymbol{\Omega}')$	°[rad]
$\boldsymbol{\Omega}(\mu, \phi)$	direction of propagation [viewing direction]		–
Ω_x	direction-cosine in x	$\sin\theta\cos\phi$	–
Ω_y	direction-cosine in y	$\sin\theta\sin\phi$	–
Ω_z	direction-cosine in z	$\cos\theta$	–
$\boldsymbol{\Omega}_0$	direction of incoming (collimated) (solar) radiation	$\boldsymbol{\Omega}(-\mu_0, \pi - \phi_0)$	–
$d\boldsymbol{\Omega}$	element of solid angle	$d\mu d\phi$	sr
$ds/d\boldsymbol{\Omega}$	differential cross-section	$\sigma_s p(\cdot)/N$	m^2/sr

2. PHYSICAL CONSTANTS

Symbol	Name	Value	Units
c	velocity of light (in vacuum)	2.99825×10^{8}	m/s
h	Planck's constant	6.62618×10^{34}	J s
k	Boltzmann's constant	1.38066×10^{23}	J/K
σ_{B}	Stefan-Boltzmann constant, $\pi \int B_{\nu}(T)\mathrm{d}\nu/T^4 = 2\pi^5 k^4/15c^2h^3$	5.67032×10^{-8}	W/m^2/K^4
$T\lambda_{\mathrm{max}}$	Wien's wavelength displacement constant, $0.20141\cdots \times hc/k$	0.28978	cm K
Tc/ν_{max}	Wien's wavenumber displacement constant, $0.35443\cdots \times hc/k$	0.50995	cm K
T_{s}	triple-point of water	273.16	K
ρ_{w}	density of liquid water (at S.T.P.)	10^3 [1]	kg/m^3 [g/cm^3]

3. SOLAR, TERRESTRIAL AND ATMOSPHERIC CONSTANTS

Symbol	Name	Value	Units
$T_\odot$	Sun's effective emission temperature	≈ 5775	K
$R_\odot$	Sun's (equatorial) radius	6.960×10^5	km
AU	(mean) Sun-Earth distance [Astronomical Unit]	1.4960×10^8	km
$2R_\odot/\mathrm{AU}$	angular diameter of Sun from Earth [31.9876 arc min]	9.3048	mrad
$\delta\Omega_\odot$	solid angle subtended by Sun from Earth, $\pi R_\odot^2/\mathrm{AU}^2$	6.799×10^{-5}	sr
F_0	(mean) solar constant, $(\sigma T_\odot^4/\pi)\delta\Omega_\odot = \sigma T_\odot^4 (R_\odot/\mathrm{AU})^2$	$\approx 1.365 \times 10^3$	W/m^2
$R_\oplus$	Earth's (equatorial) radius	6.378388×10^3	km
g	standard surface gravity	9.80665	m/s^2
p_s	standard surface pressure (N.B. 10^5 Pa = 10^3 hPa = 10^3 mbar)	1.01325	10^5 Pa [J/m^3]
R_a	specific gas constant of dry air	2.8704×10^2	J/K/kg
n_s	density of dry air (at S.T.P.)	2.686754×10^{25}	m^{-3}
ρ_s	mass density of dry air (at S.T.P.), $R_\mathrm{a} T_\mathrm{s}/p_\mathrm{s}$	1.2925	kg/m^3
C_v	constant-volume specific heat of dry air (at S.T.P.)	0.718×10^3	J/K/kg
C_p	constant-pressure specific heat of dry air (at S.T.P.), $\approx (7/5) C_\mathrm{v}$	1.005×10^3	J/K/kg
H	(nominal) scale-height of atmosphere, $R_\mathrm{a} T_\mathrm{s}/g$	7.994	km

4. SETS AND TOPOLOGY

Symbol	Name	Definition, Relation to Others
$\mathbb{N}$	all (non-negative) integers	$\{0, 1, 2, \ldots\}$
$\mathbb{Z}$	all (signed) integers	$\{\ldots, -2, -1, 0, 1, 2, \ldots\}$
$\mathbb{R}$	all real numbers	$(-\infty, +\infty)$
$\mathbb{R}^+$	non-negative real numbers	$[0, +\infty)$
$[a, b]$	closed interval of $\mathbb{R}$	$\{x \in \mathbb{R} : a \leq x \leq b\}$
(a, b)	open interval of $\mathbb{R}$	$\{x \in \mathbb{R} : a < x < b\}$
$[a, b)$	a semi-open interval of $\mathbb{R}$	$\{x \in \mathbb{R} : a \leq x < b\}$
$(a, b]$	another semi-open interval	$\{x \in \mathbb{R} : a < x \leq b\}$
Ξ	unit sphere (of direction vectors)	$\{\boldsymbol{\Omega} \in \mathbb{R}^3 : \|\boldsymbol{\Omega}\| = 1\}$
Ξ_+	upward hemisphere (of directions)	$\{\boldsymbol{\Omega}(\mu, \phi) \in \Xi : \mu \geq 0\}$
Ξ_-	downward hemisphere (of directions)	$\{\boldsymbol{\Omega}(\mu, \phi) \in \Xi : \mu \leq 0\}$
$S_1 \times S_2$	(Cartesian) product of 2 sets, e.g., $(\boldsymbol{x}, \boldsymbol{\Omega}) \in \mathbb{R}^3 \times \Xi$	
$1_S(\boldsymbol{x})$	indicator function of set S	$= 1$ if $\boldsymbol{x} \in$ S, $= 0$ otherwise
$\underline{\mathrm{S}}$	closure of a point-set S [itself *and* limits of all its infinite sequences]	$\supseteq$S, $=$S if it is closed
M	((open) convex) (optical) medium	$\subseteq \mathbb{R}^3$
∂M	boundary of a(n optical) medium	

5. MATHEMATICAL ANALYSIS

Symbol	Name	Definition, Relation to Others
$\delta q, \Delta q$	a small amount [perturbation] of quantity q	
$f_a(x), f(a;x)$	function f of (fixed) parameter a and variable x	
$\hat{f}(s), L[f](s)$	Laplace transform of $f(t)$	$\int f(t)\mathrm{e}^{-st}\mathrm{d}t$
$\vec{x}$	2D ([horizontal position]) vector	
$\tilde{f}(\mathbf{k}), F[f](\mathbf{k})$	2D Fourier transform of $f(\vec{x})$	$\int f(\vec{x})\mathrm{e}^{\pm(2\pi)\mathrm{i}\mathbf{k}\bullet\vec{x}}\mathrm{d}\vec{x}$
$f(\vec{x}), F^{-1}[\tilde{f}](\vec{x})$	inverse Fourier transform of $\tilde{f}(\mathbf{k})$ in 2D	$\int \tilde{f}(\mathbf{k})\mathrm{e}^{\mp(2\pi)\mathrm{i}\mathbf{k}\bullet\vec{x}}\,\mathrm{d}\mathbf{k}(/(2\pi)^2)$
$\boldsymbol{a}$	an arbitrary 3D vector	
$\boldsymbol{ab}$	tensor [outer] product of vectors $\boldsymbol{a}$ and $\boldsymbol{b}$	
$\boldsymbol{a}\bullet\boldsymbol{b}$	scalar [inner] product of vectors $\boldsymbol{a}$ and $\boldsymbol{b}$	Trace[$\boldsymbol{ab}$]
$a, \|\boldsymbol{a}\|$	(Euclidian) norm of vector $\boldsymbol{a}$	$(\boldsymbol{a}\bullet\boldsymbol{a})^{1/2}$
$< f, g >, (f, g)$	scalar [inner] product of functions f and g	$\int f(\vec{x})g(\vec{x})\mathrm{d}\vec{x}$
$\|f\|^2$	(L_2) norm of function f, squared	$< f, f >$
$\partial/\partial\xi, \partial_\xi$	partial derivative with respect to $\xi = t, x, y, z$ or ...	
∇	gradient [nabla] (operator)	$(\partial_x, \partial_y, \partial_z)^{\mathrm{T}}$
∇^2	Laplacian (operator)	$\nabla\bullet\nabla = \partial_x^2 + \partial_y^2 + \partial_z^2$
$\delta(\cdot)$	(Dirac) delta-function, has $1/(\cdot)^d$-units in d dimensions	
$H(\cdot), \Theta(\cdot)$	(Heaviside) step-function	integral of $\delta(\cdot)$ in d = 1
$\Gamma(a)$	(Euler's) Gamma-function $\int_0^\infty x^{a-1}\mathrm{e}^{-x}\mathrm{d}x$	$\Gamma(n+1) = n!, n \in \mathbb{N}$
$\boldsymbol{n}(\boldsymbol{x})$	(outward) (unit) normal vector (to boundary ∂M) (at $\boldsymbol{x}$)	

6. PROBABILITY AND STATISTICS

Symbol	Name	Definition, Relation to Others
$\Pr\{\cdot\}$	probability of event defined in argument	
p_i	probability of discrete event with index "i"	
$P(\cdot)$	(cumulative) probability distribution function,	a definite integral of $p(\cdot)$
$p(\cdot)$	probability density function, has 1/$(\cdot)$-units	$\pm \mathrm{d}P/\mathrm{d}(\cdot)$
$\mathcal{E}(\cdot)$	(mathematical) expectation of argument	
$\mathcal{D}(\cdot)$	variance of argument	$\mathcal{E}((\lbrack\cdot\rbrack - \mathcal{E}(\cdot))^2) = \mathcal{E}(\lbrack\cdot\rbrack^2) - \mathcal{E}(\cdot)^2$
m_f	mean of quantity f	an alternative for $\mathcal{E}(f)$
σ_f, s_f	standard deviation of quantity f	an alternative for $\mathcal{D}(f)^{1/2}$
$\overline{(\cdots)}$	spatial average of $(\cdots)$ over a domain S	$\int_S (\cdots)\mathrm{d}\vec{x} \;/\; \int_S \mathrm{d}\vec{x}$
$\langle\cdots\rangle$	spatial or ensemble average (or both)	$\int (\cdots)\mathrm{d}P(\cdots)$
$E_f(\mathbf{k})$	(wavenumber [energy] [power]) spectrum of $f(\vec{x})$	$\propto \lvert\tilde{f}(\mathbf{k})\rvert^2$
$E_f(k)$	(1D (wavenumber [etc.])) spectrum of $f(x)$	$\int E_f(\mathbf{k}')\delta(\lVert\mathbf{k}'\rVert - k)\mathrm{d}\mathbf{k}'$
β	spectral exponent	$E(k) \propto k^{-\beta}$

Index